A long-chain fatty acid elongase Elovl6 regulates mechanical damage–induced keratinocyte death and skin inflammation

Yoshiyuki Nakamura [1], Takashi Matsuzaka [2], Satoko Tahara-Hanaoka [1,3], Kazuko Shibuya [1,3], Hitoshi Shimano [2,3,4,5], Chigusa Nakahashi-Oda [1], Akira Shibuya [1,3]

Departments of [1]Immunology and [2]Internal Medicine (Endocrinology and Metabolism), Faculty of Medicine, [3]Life Science Center of Tsukuba Advanced Research Alliance (TARA), and [4]International Institute for Integrative Sleep Medicine (WPI-IIIS), University of Tsukuba, 1-1-1 Tennodai, Tsukuba, Ibaraki 305-8575, Japan
[5]AMED-CREST, Japan Agency for Medical Research and Development (AMED), 1-7-1, Ohte-machi, Chiyoda-ku, Tokyo, 100-0004, Japan

Correspondence should be addressed to Akira Shibuya (e-mail: ashibuya@md.tsukuba.ac.jp; tel: +81-29-853-3281; fax: +81-29-853-3410) or Chigusa Nakahashi-Oda (e-mail: chigusano@md.tsukuba.ac.jp; tel: +81-29-853-3281; fax: +81-29-853-3410)

This research was supported in part by grants provided by the Ministry of Education, Culture, Sports, Science, and Technology of Japan (to A.S. [16H06387, 15H01365] and C. N.-O. [16H05350]). Y.N. is a fellow of the Kibo Project of the Tadamitsu Kishimoto Foundation of the Japanese Society of Immunology.

Abstract

Mechanical damage on the skin not only affect the barrier function but also induce various immune responses, which trigger or exacerbate the inflammation in healthy individuals and patients with inflammatory skin diseases. However, how mechanical damage-induced skin inflammation is regulated remains largely unknown. Here, we show that mechanical damage due to tape stripping triggered keratinocyte death and release of danger-associated molecular patterns (DAMPs) such as high-mobility group box 1 protein (HMGB-1) and IL-1α, which induced production of proinflammatory cytokines and chemokines IL-1β and CXCL-1 by keratinocytes in mice. We also show that a long-chain fatty acid elongase Elovl6 is expressed in keratinocytes. Mice deficient in Elovl6 had increased epidermal levels of cis-vaccenic acid (CVA); this accelerated keratinocyte death triggered by tape stripping and release of DAMPs and exacerbated skin inflammation. Our results demonstrate that Elovl6 regulates mechanical damage–triggered keratinocyte death and skin inflammation.

Introduction

The mechanical damage induced by physical forces—including stretching, compression, and friction—on epithelial and endothelial cells plays a critical role in tissue homeostasis (Abe and Berk 2014; Angelini *et al.* 2012; Hofmann *et al.* 2004; Reichelt 2007; Wyatt *et al.* 2016). Under physiologic conditions, keratinocytes are the epidermal cell population most affected by mechanical damage (Reichelt 2007), which induces them to proliferate and produce cytokines. Streching of keratinocytes in vitro opens Ca^{2+} channels, resulting in the phosphorylation of Akt (Yano *et al.* 2006). This process also induces clustering and co-localization of β-integrins and epidermal growth factor receptor, followed by activation of the downstream signaling molecule extracellular signal-regulated kinase (ERK) 1/2 (Knies *et al.* 2006).

Mechanical damage not only affect the barrier function of the skin but also induce various immune responses (Verhoeven *et al.* 2008), which trigger inflammation at the site of the stress on the skin of healthy individuals. Moreover, mechanical damage on the skin exacerbates the inflammation in patients with inflammatory skin diseases. For example, scratching of itching lesions exacerbates the skin inflammation in atopic dermtitis (AD), which is called the itch-scratch cycle (Verhoeven *et al.* 2008; Verhoeven *et al.* 2009; Wahlgren 1999). In addition, scratching induces development of new skin

lesions in psoriasis, well known as the Koebner phenomenon (Köbner 1876). However, how mechanical damage-induced skin inflammation is regulated remains largely unknown.

Elongation of long-chain fatty acids family member 6 (Elovl6) is a rate-limiting microsomal enzyme that catalyzes the elongation of saturated and monounsaturated fatty acids (Saito *et al.* 2011). Elovl6 elongates palmitate (PA) (C16:0) to stearate (SA) (C18:0) and palmitoleate (POA) (C16:1n-7) to cis-vaccenic acid (CVA) (C18:1n-7) (Saito *et al.* 2011). Elovl6 is highly expressed in white adipose tissue and liver (Matsuzaka *et al.* 2002). In previous studies, mice deficient in Elovl6 (*Elovl6*$^{-/-}$ mice) had increased levels of PA in the liver and lung (Matsuzaka *et al.* 2007; Sunaga *et al.* 2013). Elovl6 is involved in metabolic diseases, such as insulin resistance (Matsuzaka *et al.* 2007) and atherogenesis (Saito *et al.* 2011), as well as inflammatory diseases, including attenuated high-fat–diet-induced hepatic inflammation (Matsuzaka *et al.* 2012) and regulated bleomycin-induced pulmonary fibrosis (Sunaga *et al.* 2013) . In addition, Elovl6 is highly expressed in skin (Matsuzaka *et al.* 2002), which is one of the most lipid-enriched organs. Lipids in the skin play crucial roles in homeostasis; they are involved in epidermal permeability and barrier function (Ishikawa *et al.* 2010), the

79 composition of microbiota (Nguyen *et al.* 2016), epithelialization (Liu *et al.* 2014), and

80 inflammation (Zhang *et al.* 2015).

81 In the current study, we examined how mechanical damage induces skin

82 inflammation and whether long-chain fatty-acid composition regulated by Elovl6 is

83 involved in mechanical damage onto the skin.

84

Results

Elovl6$^{-/-}$ mice show exacerbated mechanical damage–induced skin inflammation.

Tape stripping, which mimics scratching, is a well-established method for inducing mechanical stress or damage on the skin (Onoue *et al.* 2009; Takahashi *et al.* 2013). To investigate the role of Elovl6 in mechanical damage–induced skin inflammation, we established a mouse model of dermatitis by using repeated tape stripping twenty times, which induced the skin damage and barrier disruption. After this treatment, erythema was more severe in *Elovl6*$^{-/-}$ mice than in wild-type mice (**Figure 1A**). Moreover, the epidermis was thicker, and neutrophil infiltration was significantly greater, in *Elovl6*$^{-/-}$ mice than in wild-type mice (**Figure 1B–D**). Since *Elovl6* expression was higher in the epidermis than in the dermis **(Figure supplement 1A**), we speculated that Elovl6 is expressed in keratinocytes. Indeed, the epidermis in mice deficient in Elovl6 specifically in the keratinocytes (*Elovl6*$^{fl/fl}$ *K14*-Cre mice) showed significantly decreased Elovl6 expression (**Figure supplement 1B**). As in *Elovl6*$^{-/-}$ mice, *Elovl6*$^{fl/fl}$ *K14*-Cre mice also showed increased epidermal thickness and neutrophil infiltration after tape stripping compared with control mice (**Figure 1E, F**).

To address how Elovl6 suppressed mechanical damage-induced skin inflammation, we compared skin barrier function of *Elovl6*$^{-/-}$ mice with that of wild-type

mice. However, it was comparable between two genotypes of mice, as determined by toluidine blue skin permeability assay and a transepidermal water loss test (Sassa *et al.* 2013) (**Figure supplement 2A, B**). These results suggested that Elovl6 in the keratinocytes suppressed mechanical damage-induced skin inflammation, in which a novel mechanism might be involved.

Elovl6$^{-/-}$ mice show increased IL-1β and CXCL-1 production after mechanical damage

To investigate how Elovl6 suppressed mechanical damage-induced skin inflammation, we examined the expression levels of pro-inflammatory and anti-inflammatory cytokines and chemokines potentially involved in dermatitis (Effendy *et al.* 2000). Among them, transcript levels of *Il1b* and *Cxcl1* in epidermis were increased in both wild-type and *Elovl6*$^{-/-}$ mice after tape stripping (**Figure 2A and Figure supplement 3)**. Moreover, *Elovl6*$^{-/-}$ mice showed higher expression of *Il1b* and *Cxcl1* than did wild-type mice after tape stripping (**Figure 2A**). In accordance with these results, the concentrations of IL-1β and CXCL-1 were significantly higher in the culture supernatants of *Elovl6*$^{-/-}$ epidermis harvested from mice after tape stripping than in those from wild-type epidermis (**Figure 2B)**. These cytokine levels in the epidermis from

mice deficient in an adaptor of Toll-like receptors (TLRs) MyD88, but not TRIF, were lower than those in wild-type mice after tape stripping (**Figure 2C**). These results suggest that Elovl6 suppressed mechanical damage-induced IL-1β and CXCL-1 productions that are dependent on MyD88.

Elovl6$^{-/-}$ mice show increased keratinocyte death after mechanical damage

Since histologic analysis of the skin after tape stripping revealed greater numbers of degenerated keratinocytes in *Elovl6*$^{-/-}$ mice than in wild-type mice (**Figure 3A**), we speculated that the number of dead cells were greater in the skin of *Elovl6*$^{-/-}$ mice than in that of wild-type mice after tape stripping. Indeed, flow cytometry analysis demonstrated that, although the proportion of dead keratinocytes in the epidermis of *Elovl6*$^{-/-}$ mice was comparable with that in wild-type mice in the steady state, tape stripping enhanced keratinocyte death in *Elovl6*$^{-/-}$ mice significantly more than in wild-type mice (**Fig. 3B, C**). These results suggest that Elovl6 suppressed mechanical damage-induced keratinocyte death.

Cis-vaccenic acid (CVA) is increased in _Elovl6_$^{-/-}$ mice.

138 To investigate how keratinocytes death and the skin inflammation after tape stripping
139 were exacerbated in *Elovl6*$^{-/-}$ mice, we analyzed the fatty acid composition of the
140 epidermis of wild-type and *Elovl6*$^{-/-}$ mice. Unlike in our previous reports of increased
141 PA levels in the lung and liver of *Elovl6*$^{-/-}$ mice (Matsuzaka *et al.* 2007; Sunaga *et al.*
142 2013), PA was not increased in the epidermis (**Figure 4A**). Instead, *Elovl6*$^{-/-}$ mice had
143 significantly increased CVA levels (**Figure 4A**) and greater epidermal expression of the
144 long-chain fatty acid elongases *Elovl1*, *Elovl3*, and *Elovl5* and of the stearoyl-CoA
145 desaturase *Scd3* than did wild-type mice (**Figure 4B**). Among these, *Elovl5* and *Scd3*
146 may influence CVA generation through the elongation of POA (C16:1n-7) (Burns *et al.*
147 2012) and by the conversion of PA to POA (Guillou *et al.* 2010), respectively (**Figure**
148 **supplement 4**). These results suggest that CVA might be involved in the keratinocytes
149 death and skin inflammation after tape stripping in *Elovl6*$^{-/-}$ mice.
150
151 **CVA induces keratinocyte death.**
152 To address whether CVA is involved in keratinocyte death, we cultured a human
153 keratinocyte cell line HaCaT and primary keratinocytes derived from mice in the
154 presence of CVA. We found that CVA decreased the numbers of live cells of HaCaT
155 cells and primary keratinocytes in a dose-dependent manner (**Figure 5A, B**) and

156 increased the proportion of dead primary keratinocytes (**Figure 5C**). In contrast, neither
157 oleic acid (OA), PA, POA, SA, nor trans-vaccenic acid (TVA) influenced the number of
158 live primary keratinocytes after culture (**Figure 5A, B, D**). In addition, CVA decreased
159 the number of live peritoneal macrophages as well (**Figure supplement 5A**). CVA did
160 not affect the proliferation of HaCaT cells but instead increased the number of dead
161 cells compared with those after the addition of OA (**Figure 5E**), thus indicating that
162 treatment with CVA induced cell death of HaCaT cells. This cell death was not affected
163 by triacsin C, an inhibitor of long-chain acyl-CoA synthetases (Igal *et al.* 1997; Wang *et*
164 *al.* 2012) (**Figure supplement 5B**), suggesting that CVA itself, but not its metabolites,
165 induced death of HaCaT cells. Morphologic analyses under transmission electronic
166 microscopy demonstrated increased plasma membrane rupture without in the
167 keratinocytes after CVA treatment (**Figure supplement 5C**). In vivo, we found that
168 topical application of CVA, but not OA, at a dose of 45 mM to the dorsal skin of
169 wild-type mice increased the proportion of dead keratinocytes, as analyzed by flow
170 cytometry (**Figure 5F**). Anti-cleaved caspase-9 (CC9) antibody did not stain
171 CVA-treated dead keratinocytes (**Figure supplement 5D**). Together, these results
172 suggest that CVA induced non-apoptotic cell death. Pretreatment with necrostatin-1 or
173 necrosulfonamide, which are inhibitors of receptor-interacting protein 1 (RIP1) kinase

and mixed lineage kinase domain-like protein (MLKL), respectively, did not suppress the CVA-induced death of keratinocytes (**Figure supplement 5E**), suggesting that the cell death due to CVA likely was not necroptosis (Skrzeczynska-Moncznik *et al.* 2015; Zhao *et al.* 2017). These combined results suggest that CVA induced necrosis rather than programmed cell death of keratinocytes. In addition, treatment with inhibitors of oxidative stress (IM-54) or cyclophilin D (cyclosporine A) did not influence the cell death (**Figure supplement 5E**), suggesting that the CVA-induced necrosis of keratinocytes was independent of oxidative stress (IM-54) or cyclophilin D–mediated changes in mitochondrial permeability (Chen *et al.* 2013; Nakagawa *et al.* 2005; Zeng *et al.* 2016).

CVA increased IL-1β and CXCL-1 production.

Since CVA induced non-apoptotic cell death, we then examined whether CVA increased the release of DAMPs from dead cells. The addition of CVA, but not OA, to cultures of primary keratinocytes from wild-type mice increased the concentrations of HMGB-1 and IL-1α in the supernatants (**Figure 6A**). We further examined whether these DAMPs is involved in the increase in IL-1β and CXCL-1 expression. Stimulation of primary keratinocytes derived from wild type or *Elovl6*$^{-/-}$ mice in vitro and of the epidermis from

192 the either genotype of mice in vivo with HMGB-1 or IL-1α induced *Il1β* and *Cxcl1*, and
193 the expression levels of these cytokines transcripts did not differ between both
194 genotypes of mice (**Figure supplementary 6A, B**)**.** These results suggest that CVA
195 enhanced IL-1β and CXCL-1 production by keratinocytes via HMGB-1 or
196 IL-1α. Indeed, we found that topical application of CVA, but not OA, at a dose of 45
197 mM to the dorsal skin of wild-type mice increased the expressions of *Il1β* and *Cxcl1* in
198 the epidermis (**Figure 6B**). Finally, treatment with either antagonist of IL-1 receptor or
199 CXCR-2 intradermally and intraperitoneally reduced epidermal thickness and the
200 number of neutrophils in the skin of *Elovl6*$^{-/-}$ mice (**Figure 6C, D**). These results
201 suggest that the IL-1β and CXCL-1 produced by keratinocytes played crucial roles in
202 the exacerbation of mechanical damage-induced skin inflammation in *Elovl6*$^{-/-}$ mice.
203 Taken all together, these results suggest that tape stripping triggered keratinocyte death
204 and release of HMGB-1 and IL-1α, which then stimulated the surrounding live
205 keratinocytes to produce IL-1β and CXCL-1. Elovl6 deficiency increased the proportion
206 of CVA in the skin, which accelerated keratinocyte death triggered by tape stripping and
207 the subsequent signaling cascade to the production of IL-1β and CXCL-1, thus
208 exacerbating dermatitis (**Figure 6E**).
209
210

Discussion

Previous studies have revealed increased PA and decreased OA contents in the liver and lung of *Elovl6*$^{-/-}$ mice compared with wild-type mice (Matsuzaka *et al.* 2007; Sunaga *et al.* 2013). In the current study, we noted that the OA level in the skin of *Elovl6*$^{-/-}$ mice was decreased compared with that in wild-type mice. However, PA content did not differ between the two genotypes. Instead, epidermal levels of CVA were greater in *Elovl6*$^{-/-}$ mice than in wild-type mice, presumably owing to its efficient conversion to CVA by the concomitant induction of SCD3 and Elovl5 productions (Burns *et al.* 2012; Guillou *et al.* 2010). Although it remains unclear at present how Elovle6 regulates the fatty acid composition and the enzyme alteration in the skin, these combined results suggest that regulation of the elongation of saturated and monounsaturated fatty acids is—in part—dependent on the organs or tissues.

The biologic function of CVA has been poorly understood. Here, we demonstrated that CVA directly induced cell death in cultures of primary keratinocytes from mice. Specifically, the cells killed by CVA lacked one of the hallmarks of apoptosis, namely caspase-9 activation. In addition, morphologic analyses revealed characteristics of necrosis, including plasma membrane rupture without blebbing (Krysko *et al.* 2008) . None of the inhibitors of necroptosis, oxidative stress, or

229 cyclophilin-D-associated cell death—including necrostatin-1, NSA, IM-54, and
230 cyclosporine A—inhibited the CVA-induced cell death. In addition, triacsin-C treatment
231 failed to suppress CVA-induced cell death. These results suggest that CVA induced
232 necrosis rather than programmed cell death of keratinocytes.

233 Long-chain fatty acids elicit a variety of biologic effects, including cell death.
234 For example, PA induces apoptosis in many cell types, and this response is abrogated by
235 OA (Gillet *et al.* 2015; Sunaga *et al.* 2013). In contrast, PA induces
236 RIP1/RIP3-dependent necroptosis in RAW 264.7 cells (Kim *et al.* 2017), and (although
237 the results are controversial) OA has been reported to induce the death of various cell
238 types (Brinkmann *et al.* 2013; Moravcova *et al.* 2015). The molecular mechanisms of
239 these cytotoxic effects remain poorly understood; features proposed to be involved in
240 these toxicities include loss of membrane integrity, changes in mitochondrial
241 transmembrane potential, activation of caspase-3, and the production of reactive oxygen
242 species (Brinkmann *et al.* 2013; Fontana *et al.* 2013). In the current study, we found that,
243 beginning soon after its addition to the cultures, CVA was severely cytotoxic to HaCaT
244 cells, mouse peritoneal macrophages, and primary keratinocytes; CVA can thus be
245 added to the list of possible lipotoxins.

Previous studies have demonstrated that, compared with OA and SA, supplementation with both CVA and TVA (dose, 30 μM) significantly suppress the growth of HT-29 tumor cells after culture for 9 days (Awad *et al.* 1995). Moreover, CVA leads to greater hydrolysis of phosphoinositides in the plasma membrane than does TVA (Awad *et al.* 1995), suggesting that CVA is incorporated into the plasma membrane and affects the phospholipids composition. In the present study, we showed that CVA at concentrations of 200 μM or greater induced the death, rather than the suppression of growth, of keratinocytes, thus suggesting that the higher amount of CVA induces damage of the plasma membrane sufficiently to induce necrosis. In addition, given that TVA did not induce keratinocyte death, the cytotoxic effect of CVA may be structure dependent. Whereas trans-unsaturated fatty acids have a linear structure and can be packed regularly in the plasma membrane, cis-unsaturated fatty acids such as OA and CVA, which have a characteristic angular kink, may distort the structure of the lipid bilayer and thus destabilize the plasma membrane (Fontana *et al.* 2013). Therefore, although further studies are required to determine the detailed mechanism of CVA-induced cell death, we speculate that incorporation of CVA into the plasma membrane creates a bulky 3-dimensional structure compared with those associated with

263 other cis-monounsaturated fatty acids and thus induces cell death by disrupting the
264 plasma membrane.

265 Fatty acids reportedly play important roles in modulating dermatitis. For
266 example, a high-fat diet enriched with oleic acid impairs contact hypersensitivity
267 responses to trinitrochlorobenzene and FITC (Katagiri *et al.* 2008). In addition, oral
268 administration of docosahexaenoic acid leads to the generation of regulatory T cells,
269 which thus attenuate dinitrochlorobenzene-induced dermatitis (Han *et al.* 2015).
270 Moreover, topical or oral application of linoleic acid and TVA, which are enriched in
271 milk fat, decreases the severity of OVA-induced atopic dermatitis (Sun *et al.* 2011).

272 Atopic dermatitis (AD) is one of the most common skin diseases and is
273 characterized by pruritic and eczematous skin lesions. The outermost layer of the
274 epidermis, the stratum corneum, contains decreased levels of ceramides (very
275 long-chain fatty acids), leading to impaired barrier function in patients with AD, and the
276 average chain length of ceramide fatty acids is negatively correlated with epidermal
277 permeability in these patients (Ishikawa *et al.* 2010). Moreover, *Elovl1*$^{-/-}$ and *Elovl4*$^{-/-}$
278 mice, both of which demonstrate a global decrease in the chain length of ceramide fatty
279 acids of the stratum corneum, show impaired barrier function (Li *et al.* 2007; Sassa *et al.*
280 2013). Mechanical stress, such as scratching, increases the severity of AD by removing

281 the stratum corneum (thus diminishing the epidermal barrier function) and by inducing
282 the production of pro-inflammatory cytokines (Verhoeven *et al.* 2008; Wahlgren 1999).
283 On the other hand, psoriasis is characterized by well-demarcated scaly erythema and
284 plaque, which sometimes show itching, and histopathologically, these lesions reveal
285 hyperproliferation of keratinocytes and neutrophil infiltration (Hirotsu *et al.* 2012). The
286 skin lesions of psoriasis are well-known to be triggered or exacerbated, as the Koebner
287 phenomenon, by mechanical stress (Köbner 1876). Our current results suggest that
288 Elovl6 may regulates mechanical stress-induced exacerbation of skin inflammation due
289 to inhibition of keratinocyte death by CVA in patients with AD and psoriasis.
290
291

292 **Materials and Methods**

293 **Mice.** *Elovl6*$^{-/-}$ mice on the C57BL/6J background were described previously
294 (Matsuzaka *et al.* 2007). C57BL/6J mice raised under specific pathogen-free conditions
295 were purchased from Clea Japan (Tokyo, Japan). Germ-free mice were bred and
296 maintained in isolators at Sankyo Laboratories (Tsukuba, Japan), and their germ-free
297 status was routinely confirmed by in-house aerobic and anaerobic culture of feces.
298 *K14*-Cre, *Ticam1*$^{-/-}$, and *Myd88*$^{-/-}$ mice on the B57BL/6 background were purchased
299 from Jackson Laboratories (Bar Harbor, Maine, USA). *Elovl6*$^{fl/fl}$ mice were crossed with
300 *K14*-Cre transgenic mice to generate Elovl6-knockout mice specifically in keratinocytes
301 (*Elovl6*$^{fl/fl}$ *K14*-Cre). Mice between 8 and 10 weeks of age were used for the
302 experiments. All experiments were performed in accordance with the guidelines of the
303 animal ethics committee of the University of Tsukuba Animal Research Center.
304
305 **Tape stripping (Nakajima *et al.* 2012).** To generate mechanical damage-induced
306 dermatitis, a 2.5×2.5 cm area of the dorsal skin was shaved and tape-stripped 20 times
307 by using adhesive tape (Johnson and Johnson); a 1×1-cm piece of sterile gauze
308 moistened with 100 µl PBS was placed on the shaved skin and secured with transparent
309 bio-occlusive tape (Tegaderm Roll, 3M, Maplewood, Minnesota, USA) to prevent the

mice from licking the area. These procedures were repeated every other day until analysis.

Cytokine measurement of epidermis or cultured keratinocytes. Dorsal skin samples before and after tape stripping were resected from adult mice and incubated in RPMI medium in the presence of dispase II (3 mg/ml) (Wako Pure Chemical, Osaka, Japan) for 1 h at 37 °C under 5% CO_2. The epidermis was then separated from the dermis under a stereomicroscope. Samples of epidermis (diameter, 4 mm) were cultured in 50 μl of DMEM containing 10% FBS in a 96-well plate at 37 °C under 5% CO_2 for 24 h and the concentrations of IL-1β, CXCL-1, TNFα, and IL-10 in the culture supernatants were measured by using cytometric bead arrays (CBA) (BD Biosciences) according to the manufacturer's protocol. The skin of new born mice (younger than 3 days old) was incubated in CnT-07 medium (CELLnTEC Advanced Cell Systems) in the presence of dispase II (1mg/ml) (CELLnTEC Advanced Cell Systems) at 4 °C for 16 h. The epidermis was isolated from the skin and incubated in Accutase (CellnTEC Advanced Cell Systems) at room temperature for 20 min. The keratinocytes collected were maintained in CnT-07 medium (CELLnTEC Advanced Cell Systems) according to the manufacturer's protocol. Keratinocytes were then stimulated with long-chain fatty

328 acids at 37 °C under 5% CO_2 for 10 h and the culture supernatants were analyzed for
329 IL-1α and HMBG-1 by flow cytometry using cytokine beads array (CBA) and for
330 HMGB-1 using an ELISA KIT II (Shino-test Corporation). Keratinocytes were also
331 stimulated with IL-1α or HMGB-1 at 37 °C under 5% CO_2 for 3 h and analyzed for *Il1b*
332 and *Cxcl1* by quantitative real-time PCR analysis (qRT-PCR).
333
334 **qRT-PCR.** Total RNA was isolated by using ISOGEN (Wako Pure Chemical).
335 Quantitative real-time PCR analysis was performed on a 7500 Fast Real-Time PCR
336 System (Applied Biosystems, Foster City, California, USA) with Power SYBR Green
337 PCR Master Mix (Applied Biosystems). Results are presented relative to those of the
338 housekeeping gene encoding GAPDH (*gapdh*). Primers used were as follows: *Il1b* fwd,
339 GAAATGCCACCTTTTGACAGTG; *Il1b* rev, TGGATGCTCTCATCAGGACAG;
340 *Cxcl1* fwd, CTGGGATTCACCTCAAGAACATC; *Cxcl1* rev,
341 CAGGGTCAAGGCAAGCCTC; *Ccl2* fwd, CAGGTCCCTGTCATGCTTC; *Ccl2* rev
342 ATGAGTAGCAGCAGGTGAGTG; *Elovl6* fwd, ACAATGGACCTGTCAGCAAA;
343 *Elovl6* rev, GTACCAGTGCAGGAAGATCAGT; *Tnfa* fwd,
344 CCTGTAGCCCACGTCGTAG; *Tnfa* rev, GGGAGTAGACAAGGTACAACCC; *Il1a*
345 fwd, AGGGAGTCAACTCATTGGCG; *Il1a* rev, TGGCAGAACTGTAGTCTTCGT; *Il6*

rev, TCCACGATTTCCCAGAGAAC; *Il10* fwd, GCTGGACAACATACTGCTAACC; *Il10* rev, ATTTCCGATAAGGCTTGGCAA; *Il33* fwd, GGTGAACATGAGTCCCATCA; *Il33* rev, CGTCACCCCTTTGAAGCTC; *Tgfb* fwd, TGACGTCACTGGAGTTGTACGG; *Tgfb* rev, GGTTCATGTCATGGATGGTGC; *Ccl2* rev ATGAGTAGCAGCAGGTGAGTG; *Ifng* fwd, ACAGCAAGGCGAAAAAGGATG; *Ifng* rev, TGGTGGACCACTCGGATGA; *Il4* fwd; ATCATCGGCATTTTGAACGAGG; *Il4* rev; TGCAGCTCCATGAGAACACTA; *Il17* fwd, TTTAACTCCCTTGGCGCAAAA; *Il17* rev, CTTTCCCTCCGCATTGACAC; *Elovl1* fwd, TCCAAAGCTACCCTCTGATGG; *Elovl1* rev, AGGGAGAGTATCACCAGTGAGA; *Elovl2* fwd, ACGCTGGTCATCCTGTTCTT; *Elovl2* rev, GCCACAATTAAGTGGGCTTT; *Elovl3* fwd, TTCTCACGCGGGTTAAAAATGG; *Elovl3* rev, GAGCAACAGATAGACGACCAC; *Elovl4* fwd, GCCCTGTGGTGGTATTTTGT; *Elovl4* rev, TGGTGGTACACGTGAAGGAA; *Elovl5* fwd, GGTGGCTGTTCTTCCAGATT , *Elovl5* rev, CCCTTCAGGTGGTCTTTCC, *Elovl6* fwd, ACAATGGACCTGTCAGCAAA; *Elovl6* rev, GTACCAGTGCAGGAAGATCAGT; *Elovl7* fwd, CATCGAGGACTGTGCGTTTTT; *Elovl7* rev, CCAGGATGATGGTTTGTGGCA; *Scd1* fwd,

364 TCAACTTCACCACGTTCTTCA; *Scd1* rev, CTCCCGTCTCCAGTTCTCTT; *Scd2*

365 fwd, TGGTTTCCATGGGAGCTG; *Scd2* rev, TTGATGTGCCAGCGGTACT; *Scd3*

366 fwd, CTGACCTGAAAGCCGAGAAG; *Scd3* rev, GCAGAATGCCAGGCTTGTA;

367 *Gapdh* fwd, AGGTCGGTGTGAACGGATTTG; and *Gapdh* rev

368 TGTAGACCATGTAGTTGAGGTCA.

369

370 **Histology.** For histologic analysis, mouse skin was fixed in 10% formalin, embedded in

371 paraffin, sectioned, and stained with hematoxylin and eosin. For analysis of epidermal

372 thickness or cell number, 18 randomly selected sites were evaluated by using light

373 microscopy or fluorescent microscopy (MZ-X710, Keyence, Osaka, Japan) and its

374 associated software.

375

376 **Analysis of cleaved caspase-9.** Cells were treated or not with CVA or UV (180 mJ/

377 cm^2 for 3 min) and then fixed with 4% paraformaldehyde for 15 min and then with 5 %

378 BSA in PBS containing 0.3% Triton X-100 for 1 h. Subsequently, cells were incubated

379 with rabbit anti-cleaved caspase-9 antibody (1:200; Cell Signaling) for 1 h at room

380 temperature, followed by incubation with Alexa Fluor 594-conjugated donkey

anti-rabbit IgG (1:200; Thermo Fisher Scientific) secondary antibody for 30 min. Finally, cells were counterstained with DAPI.

Cell death and proliferation analyses. Primary keratinocytes from neonatal epidermis, prepared as described above, or human HaCaT cells were maintained in CnT-07 medium, as described above, and DMEM with 10% FBS, respectively, at 37 °C under 5% CO_2. Peritoneal macrophages were harvested by lavage of the peritoneal cavity and suspended in DMEM containing 10% FBS. Primary keratinocytes and HaCaT cells and peritoneal macrophages were seeded onto 48-well plates at a density of 1×10^5 cells and 2×10^5 cells/ well, respectively. After incubation at 37 °C for 2 h, the cells were washed with PBS three times to remove unattached cells and stimulated with different concentrations of free fatty acids dissolved in ethanol (final dose of 100 ~ 500 μM), including oleic acid (OA), palmitic acid (PA), stearic acid (SA), palmitoleic acid (POA) (Wako Pure Chemical), trans-vaccenic acid (TVA) or cis-vaccenic acid (CVA) (Sigma-Aldrich). To block specific types of cell death or inhibit long-chain acyl-coenzyme A synthetase, cells were pretreated with 1 mM of necrostatin-1 (Cayman Chemicals), 1 mM of necrosulfonamide (Cellagen Technology), 2 mM of IM-54 (Sigma

Aldrich), 1 mM of cyclosporine A (Sigma Aldrich), or 10 μM of triacsin C (Abcam) for 6 h before fatty acid stimulation.

For proliferation assay, these cells were stained or not with 10 μM of CFSE (Invitrogen) for 5min at 37°C before fatty acid stimulation, according to the manufacturer instructions. Cells were then stained with propidium iodine (PI) and analyzed for PI-positive and -negative cell populations and CFSE dilution by flow cytometry. For the analysis of cell death in vivo, skin tissue was incubated in 0.5% trypsin (Wako) in PBS, and separated into epidermis. Epidermal cells were stained with CD45.2 (clone:104, BD pharmingen), CD49f (clone: GoH3, Miltenyi Biotec) and PI, and then analyzed by flow cytometry.

Transmission electron microscopy. Cultured keratinocytes were fixed by incubating 2.5% glutaraldehyde in PBS (pH 7.4) at 4 °C overnight, postfixed in 1% osmium tetraoxide at 4 °C for 30 min, and then dehydrated through graded concentrations of ethanol. Cells were then transferred to propylene oxide and embedded (Poly/Bed 812, Polysciences, Warrington, Pennsylvania, USA). The samples were analyzed by electron microscopy (JEM-1400, JEOL, Peabody, Massachusetts, USA).

416 **Cytokine stimulation**. Primary mouse keratinocytes were stimulated with bovine
417 HMGB-1 (Chondrex, Redmond, Washington, USA) or mouse IL-1α (Miltenyi Biotec,
418 Bergisch Gladbach, Germany). For stimulation of keratinocytes in vitro, primary
419 keratinocytes were stimulated 500ng/ml of bovine HMGB-1 or mouse IL-1α. For
420 stimulation of keratinocytes in vivo, 200 ng of bovine HMGB-1 or mouse IL-1α in 50
421 µl PBS was injected intradermally.
422
423 **Fatty acid composition**. Lipids from mouse epidermis were extracted by using the
424 method of Bligh and Dyer (Breil *et al.* 2017). In brief, epidermis was extracted with
425 chloroform/ methanol (1:2, v/v) solution. One molar NaCl solution and chloroform were
426 added to break the monophase and incubated on ice for 10 min. After centrifugation at
427 300 G for 5 min, aqueous solution was discarded and the phase of chloroform was
428 evaporated using nitrogen gas. Following the addition of acetonitrile/ 6N HCl (90/10,
429 v/v), samples were incubated at 100 °C for 45 min. Finally, liquid-liquid extraction
430 (Milne and Zhitomirsky 2018) with ethyl acetate was performed and the reconstituted
431 samples were injected into an optimized LC/ MS/MS system. The relative abundance of
432 each fatty acid was quantified by gas chromatography.
433

434 **Transepidermal water loss (TEWL) test.** Fetuses obtained at E13.5 and E17.5 were
435 incubated in methanol for 5 min and rinsed in PBS, followed by incubation with 0.1%
436 toluidine blue for 24 h. After staining, fetuses were rinsed with PBS and the staining
437 intensity was evaluated (Sassa *et al.* 2013). TEWL was also measured on the dorsal skin
438 of wild-type and *Elovl6*$^{-/-}$ mice between 8 and 10 weeks of age by Tewameter® TM 300
439 (Integral) before and after tape stripping (Sassa *et al.* 2013). Measurements were
440 performed in triplicate for each mouse.
441
442 **Antagonist treatment.** To neutralize the IL-1 receptor, mice received 200 µl of the IL-1
443 receptor antagonist anakinra (10 mg/ml) (Kineret, Swedish Orphan Biovitrum)
444 intradermally and 300 µl of the same concentration of the antagonist intraperitoneally
445 daily during the induction of dermatitis by the mechanical stress or OVA treatment. To
446 block CXCR-2, mice received 200 µl of a CXCR-2 antagonist (0.25 mg/ml in PBS
447 containing 1% DMSO) (SB225002, Cayman Chemical, Ann Arbor, Michigan, USA)
448 intradermally and 150 µg of the same antagonist (0.5 mg/ml in PBS containing 1%
449 DMSO) intraperitoneally daily during the induction of dermatitis by the mechanical
450 stress.
451

452 **Statistical analyses.** Statistical analyses were performed by using an unpaired,

453 two-tailed Student's *t*-test (GraphPad Prism 6, GraphPad Software, La Jolla, USA). A *P*

454 value less than 0.05 was considered to be statistically significant.

455 **Acknowledgments**

456 We thank S. Mitsuishi and Y. Nomura for their secretarial assistance.

457

458 **References**

459 Abe, J., and B. C. Berk. 2014. Novel mechanisms of endothelial mechanotransduction.
460 Arterioscler Thromb Vasc Biol 34:2378-2386
461 Angelini, T. E., A. C. Dunn, J. M. Uruena, D. J. Dickrell, 3rd, D. L. Burris, and W. G.
462 Sawyer. 2012. Cell friction. Faraday Discuss 156:31-39; discussion 87-103
463 Awad, A. B., T. Herrmann, C. S. Fink, and P. J. Horvath. 1995. 18:1 n7 fatty acids
464 inhibit growth and decrease inositol phosphate release in HT-29 cells compared to n9
465 fatty acids. Cancer Lett 91:55-61
466 Breil, C., M. Abert Vian, T. Zemb, W. Kunz, and F. Chemat. 2017. "Bligh and Dyer"
467 and Folch Methods for Solid-Liquid-Liquid Extraction of Lipids from Microorganisms.
468 Comprehension of Solvatation Mechanisms and towards Substitution with Alternative
469 Solvents. Int J Mol Sci 18
470 Brinkmann, C. R., S. Thiel, and D. E. Otzen. 2013. Protein-fatty acid complexes:
471 biochemistry, biophysics and function. FEBS J 280:1733-1749
472 Burns, T. A., A. K. Kadegowda, S. K. Duckett, S. L. Pratt, and T. C. Jenkins. 2012.
473 Palmitoleic (16:1 cis-9) and cis-vaccenic (18:1 cis-11) acid alter lipogenesis in bovine
474 adipocyte cultures. Lipids 47:1143-1153
475 Chen, B., M. Xu, H. Zhang, J. X. Wang, P. Zheng, L. Gong, G. J. Wu, and T. Dai. 2013.
476 Cisplatin-induced non-apoptotic death of pancreatic cancer cells requires mitochondrial
477 cyclophilin-D-p53 signaling. Biochem Biophys Res Commun 437:526-531
478 Effendy, I., H. Loffler, and H. I. Maibach. 2000. Epidermal cytokines in murine
479 cutaneous irritant responses. J Appl Toxicol 20:335-341
480 Fontana, A., B. Spolaore, and P. Polverino de Laureto. 2013. The biological activities of
481 protein/oleic acid complexes reside in the fatty acid. Biochim Biophys Acta
482 1834:1125-1143
483 Gillet, C., D. Spruyt, S. Rigutto, A. Dalla Valle, J. Berlier, C. Louis, C. Debier, N.
484 Gaspard, W. J. Malaisse, V. Gangji, and J. Rasschaert. 2015. Oleate Abrogates
485 Palmitate-Induced Lipotoxicity and Proinflammatory Response in Human Bone
486 Marrow-Derived Mesenchymal Stem Cells and Osteoblastic Cells. Endocrinology
487 156:4081-4093
488 Guillou, H., D. Zadravec, P. G. Martin, and A. Jacobsson. 2010. The key roles of
489 elongases and desaturases in mammalian fatty acid metabolism: Insights from
490 transgenic mice. Prog Lipid Res 49:186-199
491 Han, S. C., D. H. Koo, N. J. Kang, W. J. Yoon, G. J. Kang, H. K. Kang, and E. S. Yoo.
492 2015. Docosahexaenoic Acid Alleviates Atopic Dermatitis by Generating Tregs and

493 IL-10/TGF-beta-Modified Macrophages via a TGF-beta-Dependent Mechanism. J
494 Invest Dermatol 135:1556-1564
495 Hirotsu, C., M. Rydlewski, M. S. Araujo, S. Tufik, and M. L. Andersen. 2012. Sleep
496 loss and cytokines levels in an experimental model of psoriasis. PLoS One 7:e51183
497 Hofmann, M., J. Zaper, A. Bernd, J. Bereiter-Hahn, R. Kaufmann, and S. Kippenberger.
498 2004. Mechanical pressure-induced phosphorylation of p38 mitogen-activated protein
499 kinase in epithelial cells via Src and protein kinase C. Biochem Biophys Res Commun
500 316:673-679
501 Igal, R. A., P. Wang, and R. A. Coleman. 1997. Triacsin C blocks de novo synthesis of
502 glycerolipids and cholesterol esters but not recycling of fatty acid into phospholipid:
503 evidence for functionally separate pools of acyl-CoA. Biochem J 324 (Pt 2):529-534
504 Ishikawa, J., H. Narita, N. Kondo, M. Hotta, Y. Takagi, Y. Masukawa, T. Kitahara, Y.
505 Takema, S. Koyano, S. Yamazaki, and A. Hatamochi. 2010. Changes in the ceramide
506 profile of atopic dermatitis patients. J Invest Dermatol 130:2511-2514
507 Köbner, H. 1876. Zur Aetiologie Psoriasis. Vjschr Dermatol 3:559
508 Katagiri, K., S. Arakawa, and R. Kurahashi. 2008. IL-4 restores impaired contact
509 hypersensitivity response in obese mice fed a high-fat diet enriched with oleic acid. J
510 Invest Dermatol 128:735-737
511 Kim, S. K., M. Yun, G. Seo, J. Y. Lee, and S. B. Lee. 2017. Palmitate induces
512 RIP1/RIP3-dependent necrosis via MLKL-mediated pore formation in the plasma
513 membrane of RAW 264.7 cells. Biochem Biophys Res Commun 482:359-365
514 Knies, Y., A. Bernd, R. Kaufmann, J. Bereiter-Hahn, and S. Kippenberger. 2006.
515 Mechanical stretch induces clustering of beta1-integrins and facilitates adhesion. Exp
516 Dermatol 15:347-355
517 Krysko, D. V., T. Vanden Berghe, K. D'Herde, and P. Vandenabeele. 2008. Apoptosis
518 and necrosis: detection, discrimination and phagocytosis. Methods 44:205-221
519 Li, W., R. Sandhoff, M. Kono, P. Zerfas, V. Hoffmann, B. C. Ding, R. L. Proia, and C. X.
520 Deng. 2007. Depletion of ceramides with very long chain fatty acids causes defective
521 skin permeability barrier function, and neonatal lethality in ELOVL4 deficient mice. Int
522 J Biol Sci 3:120-128
523 Liu, M., K. Saeki, T. Matsunobu, T. Okuno, T. Koga, Y. Sugimoto, C. Yokoyama, S.
524 Nakamizo, K. Kabashima, S. Narumiya, T. Shimizu, and T. Yokomizo. 2014.
525 12-Hydroxyheptadecatrienoic acid promotes epidermal wound healing by accelerating
526 keratinocyte migration via the BLT2 receptor. J Exp Med 211:1063-1078
527 Matsuzaka, T., A. Atsumi, R. Matsumori, T. Nie, H. Shinozaki, N. Suzuki-Kemuriyama,
528 M. Kuba, Y. Nakagawa, K. Ishii, M. Shimada, K. Kobayashi, S. Yatoh, A. Takahashi, K.

529 Takekoshi, H. Sone, N. Yahagi, H. Suzuki, S. Murata, M. Nakamuta, N. Yamada, and H.
530 Shimano. 2012. Elovl6 promotes nonalcoholic steatohepatitis. Hepatology
531 56:2199-2208
532 Matsuzaka, T., H. Shimano, N. Yahagi, T. Kato, A. Atsumi, T. Yamamoto, N. Inoue, M.
533 Ishikawa, S. Okada, N. Ishigaki, H. Iwasaki, Y. Iwasaki, T. Karasawa, S. Kumadaki, T.
534 Matsui, M. Sekiya, K. Ohashi, A. H. Hasty, Y. Nakagawa, A. Takahashi, H. Suzuki, S.
535 Yatoh, H. Sone, H. Toyoshima, J. Osuga, and N. Yamada. 2007. Crucial role of a
536 long-chain fatty acid elongase, Elovl6, in obesity-induced insulin resistance. Nat Med
537 13:1193-1202
538 Matsuzaka, T., H. Shimano, N. Yahagi, T. Yoshikawa, M. Amemiya-Kudo, A. H. Hasty,
539 H. Okazaki, Y. Tamura, Y. Iizuka, K. Ohashi, J. Osuga, A. Takahashi, S. Yato, H. Sone,
540 S. Ishibashi, and N. Yamada. 2002. Cloning and characterization of a mammalian fatty
541 acyl-CoA elongase as a lipogenic enzyme regulated by SREBPs. J Lipid Res
542 43:911-920
543 Milne, J., and I. Zhitomirsky. 2018. Application of octanohydroxamic acid for
544 liquid-liquid extraction of manganese oxides and fabrication of supercapacitor
545 electrodes. J Colloid Interface Sci 515:50-57
546 Moravcova, A., Z. Cervinkova, O. Kucera, V. Mezera, D. Rychtrmoc, and H. Lotkova.
547 2015. The effect of oleic and palmitic acid on induction of steatosis and cytotoxicity on
548 rat hepatocytes in primary culture. Physiol Res 64 Suppl 5:S627-636
549 Nakagawa, T., S. Shimizu, T. Watanabe, O. Yamaguchi, K. Otsu, H. Yamagata, H.
550 Inohara, T. Kubo, and Y. Tsujimoto. 2005. Cyclophilin D-dependent mitochondrial
551 permeability transition regulates some necrotic but not apoptotic cell death. Nature
552 434:652-658
553 Nakajima, S., B. Z. Igyarto, T. Honda, G. Egawa, A. Otsuka, M. Hara-Chikuma, N.
554 Watanabe, S. F. Ziegler, M. Tomura, K. Inaba, Y. Miyachi, D. H. Kaplan, and K.
555 Kabashima. 2012. Langerhans cells are critical in epicutaneous sensitization with
556 protein antigen via thymic stromal lymphopoietin receptor signaling. J Allergy Clin
557 Immunol 129:1048-1055 e1046
558 Nguyen, M. T., D. Hanzelmann, T. Hartner, A. Peschel, and F. Gotz. 2016. Skin-Specific
559 Unsaturated Fatty Acids Boost the Staphylococcus aureus Innate Immune Response.
560 Infect Immun 84:205-215
561 Onoue, A., K. Kabashima, M. Kobayashi, T. Mori, and Y. Tokura. 2009. Induction of
562 eosinophil- and Th2-attracting epidermal chemokines and cutaneous late-phase reaction
563 in tape-stripped skin. Exp Dermatol 18:1036-1043

564 Reichelt, J. 2007. Mechanotransduction of keratinocytes in culture and in the epidermis.
565 Eur J Cell Biol 86:807-816
566 Saito, R., T. Matsuzaka, T. Karasawa, M. Sekiya, N. Okada, M. Igarashi, R. Matsumori,
567 K. Ishii, Y. Nakagawa, H. Iwasaki, K. Kobayashi, S. Yatoh, A. Takahashi, H. Sone, H.
568 Suzuki, N. Yahagi, N. Yamada, and H. Shimano. 2011. Macrophage Elovl6 deficiency
569 ameliorates foam cell formation and reduces atherosclerosis in low-density lipoprotein
570 receptor-deficient mice. Arterioscler Thromb Vasc Biol 31:1973-1979
571 Sassa, T., Y. Ohno, S. Suzuki, T. Nomura, C. Nishioka, T. Kashiwagi, T. Hirayama, M.
572 Akiyama, R. Taguchi, H. Shimizu, S. Itohara, and A. Kihara. 2013. Impaired epidermal
573 permeability barrier in mice lacking elovl1, the gene responsible for very-long-chain
574 fatty acid production. Mol Cell Biol 33:2787-2796
575 Skrzeczynska-Moncznik, J., M. Bzowska, A. Nogiec, A. Sroka, M. Zarebski, L.
576 Vallieres, and K. Guzik. 2015. Rapid externalization of 27-kDa heat shock protein
577 (HSP27) and atypical cell death in neutrophils treated with the sphingolipid analog drug
578 FTY720. J Leukoc Biol 98:591-599
579 Sun, X., J. Zhang, A. K. Macgibbon, P. Black, and G. W. Krissansen. 2011. Bovine milk
580 fat enriched in conjugated linoleic and vaccenic acids attenuates allergic dermatitis in
581 mice. Clin Exp Allergy 41:729-738
582 Sunaga, H., H. Matsui, M. Ueno, T. Maeno, T. Iso, M. R. Syamsunarno, S. Anjo, T.
583 Matsuzaka, H. Shimano, T. Yokoyama, and M. Kurabayashi. 2013. Deranged fatty acid
584 composition causes pulmonary fibrosis in Elovl6-deficient mice. Nat Commun 4:2563
585 Takahashi, T., Y. Kimura, K. Niwa, Y. Ohmiya, T. Fujimura, K. Yamasaki, and S. Aiba.
586 2013. In vivo imaging demonstrates ATP release from murine keratinocytes and its
587 involvement in cutaneous inflammation after tape stripping. J Invest Dermatol
588 133:2407-2415
589 Verhoeven, E. W., S. de Klerk, F. W. Kraaimaat, P. C. van de Kerkhof, E. M. de Jong,
590 and A. W. Evers. 2008. Biopsychosocial mechanisms of chronic itch in patients with
591 skin diseases: a review. Acta Derm Venereol 88:211-218
592 Verhoeven, E. W., F. W. Kraaimaat, E. M. de Jong, J. Schalkwijk, P. C. van de Kerkhof,
593 and A. W. Evers. 2009. Individual differences in the effect of daily stressors on
594 psoriasis: a prospective study. Br J Dermatol 161:295-299
595 Wahlgren, C. F. 1999. Itch and atopic dermatitis: an overview. J Dermatol 26:770-779
596 Wang, H. W., J. S. Fang, X. Kuang, L. Y. Miao, C. Wang, G. L. Xia, M. L. King, and J.
597 Zhang. 2012. Activity of long-chain acyl-CoA synthetase is required for maintaining
598 meiotic arrest in Xenopus laevis. Biol Reprod 87:74

599 Wyatt, T., B. Baum, and G. Charras. 2016. A question of time: tissue adaptation to
600 mechanical forces. Curr Opin Cell Biol 38:68-73
601 Yano, S., M. Komine, M. Fujimoto, H. Okochi, and K. Tamaki. 2006. Activation of Akt
602 by mechanical stretching in human epidermal keratinocytes. Exp Dermatol 15:356-361
603 Zeng, F., J. P. Sherry, and N. C. Bols. 2016. Evaluating the toxic potential of
604 benzothiazoles with the rainbow trout cell lines, RTgill-W1 and RTL-W1. Chemosphere
605 155:308-318
606 Zhang, Y., Q. Li, E. Rao, Y. Sun, M. E. Grossmann, R. J. Morris, M. P. Cleary, and B. Li.
607 2015. Epidermal Fatty Acid binding protein promotes skin inflammation induced by
608 high-fat diet. Immunity 42:953-964
609 Zhao, W., H. Feng, W. Sun, K. Liu, J. J. Lu, and X. Chen. 2017. Tert-butyl
610 hydroperoxide (t-BHP) induced apoptosis and necroptosis in endothelial cells: Roles of
611 NOX4 and mitochondrion. Redox Biol 11:524-534
612

613

614 **Figures and legends**

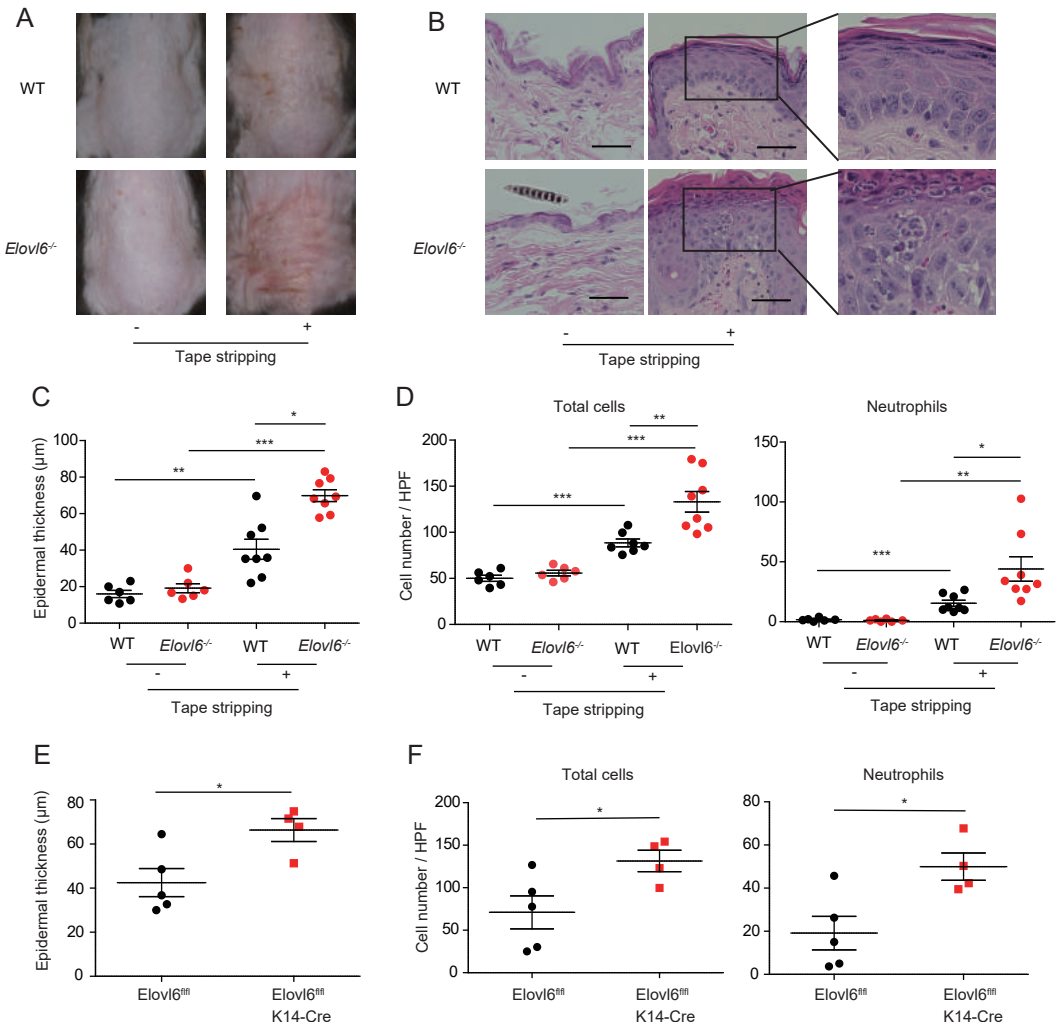

615 **Fig. 1. *Elovl6*$^{-/-}$ mice show exacerbation of dermatitis**.

616 (A to D) Representative gross findings (A), histology (hematoxylin and eosin staining)
617 (B), epidermal thickness (C), and numbers of total infiltrating cells and neutrophils in
618 the dorsal skin (D) of wild-type (n =6 or 8) and *Elovl6*$^{-/-}$ (n =6 or 8) mice before and on
619 day 9 after the start of tape stripping. (E, F) Epidermal thickness (E) and numbers of
620 total infiltrating cells and neutrophils in the skin (F) of *Elovl6*$^{fl/fl}$ (n = 5) and
621 *Elovl6*$^{fl/fl}$*K14*-Cre (n = 4) on day 9 after the start of tape stripping. Black bars indicate
622 scale (50 μm) (B). Error bars indicate 1 SD; *, P<0.05; **, P < 0.01; ***, P < 0.001.
623 Data are representative of three (A-D) and two (E, F) independent experiments.

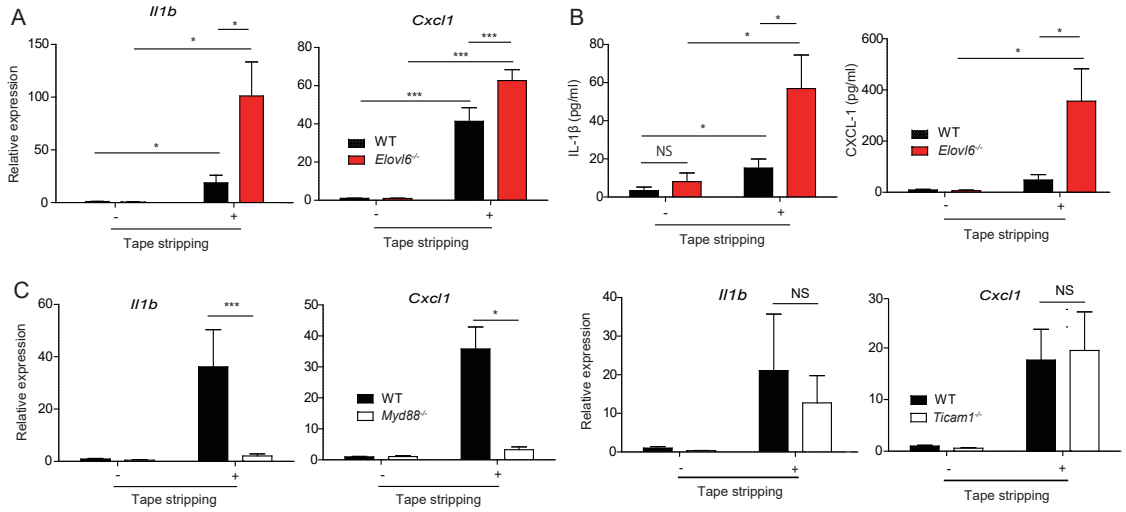

Fig. 2. Elovl6 suppresses mechanical damage-induced IL-1β and CXCL-1 production

(A) Quantitative RT-PCR analysis of epidermis of wild-type and *Elovl6*$^{-/-}$ mice isolated 6 h after tape stripping (n = 10 in each group). (B) Epidermis was isolated before, and 12 h after, tape stripping from wild-type and *Elovl6*$^{-/-}$ mice and cultured for 24 h. The concentrations of IL-1β and CXCL-1 in the supernatants were measured by using cytometric bead array (n = 11 per group). (C) Quantitative RT-PCR analysis of *Il1β* and *Cxcl1* in the epidermis of wild-type, *Myd88*$^{-/-}$, and *Ticam1*$^{-/-}$ mice before, and 6 h after, tape stripping (n = 7 to 11 per group). Error bars indicate 1 SD; *, $P<0.05$; ***, $P < 0.001$. Data are representative of three independent experiments.

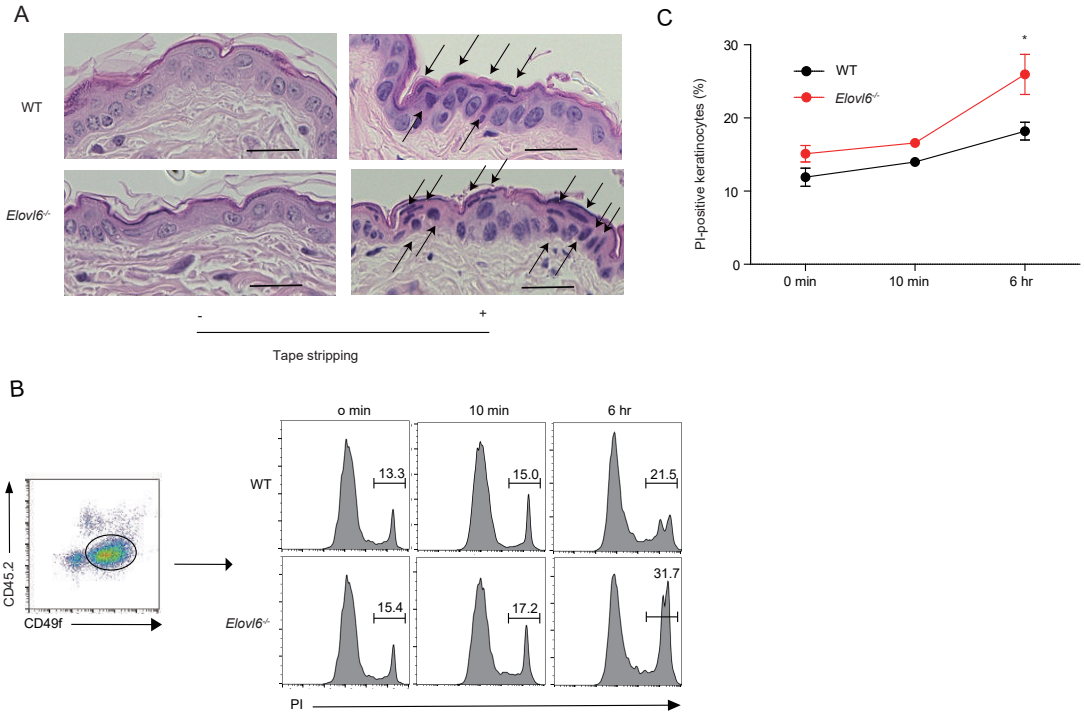

638
639
640 **Fig. 3. Elovl6 suppressed mechanical damage-induced keratinocyte death.**
641 (A) Representative histopathology of wild-type and *Elovl6*$^{-/-}$ mice 4 h after tape
642 stripping. Black arrows indicate degenerated keartinocytes with irregularly shaped
643 nuclei. Scale bar, 50 μm. (B, C) Flow cytometry of epidermal cells isolated from the
644 skin of wild-type and *Elovl6*$^{-/-}$ mice at the indicated time points after tape stripping.
645 Cells were stained with anti-CD45.2, anti-CD49f and propidium iodide (PI) and the
646 proportion of PI^{+} cells in CD45.2-CD49f+ cells were shown (n = 6 to 10 per group).
647 Error bars indicate 1 SD; *, $P < 0.05$. Data are representative of two independent
648 experiments.
649
650

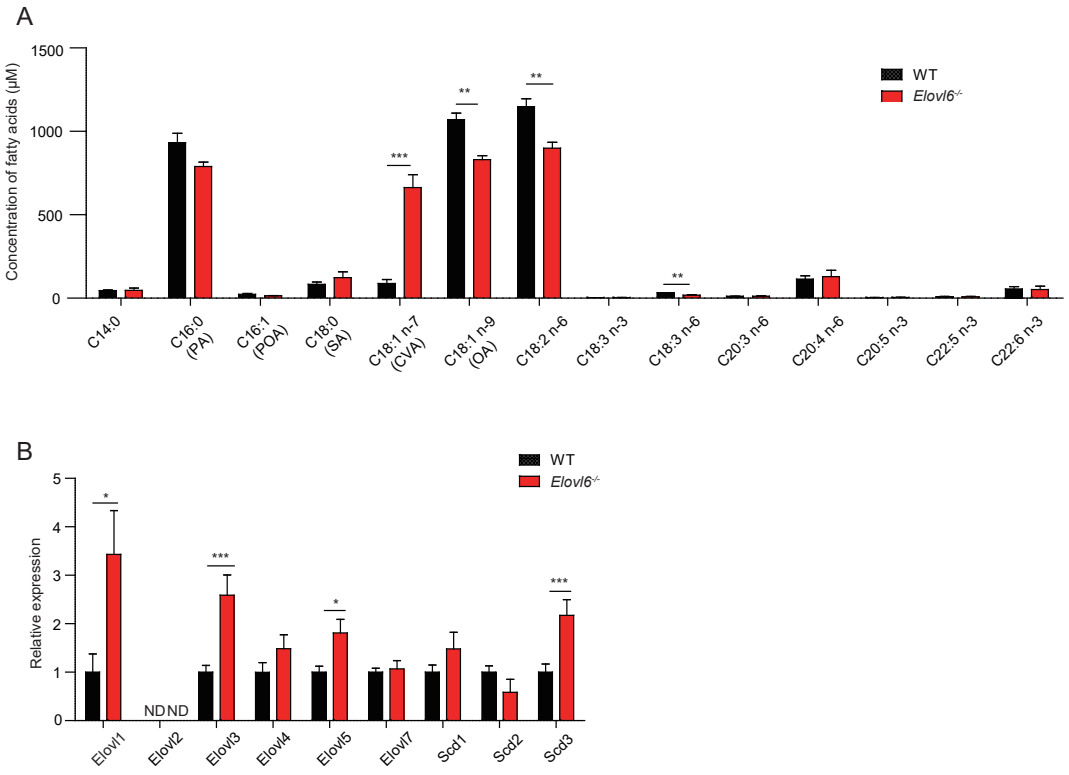

Fig. 4. Elovl6 suppressed cis-vaccenic acid production in keratinocytes.

(A) Fatty acid composition of epidermis in wild-type and *Elovl6*$^{-/-}$ mice (n = 4 per group). (B) Quantitative RT-PCR analysis of the epidermis for the expression of long-chain fatty acid elongases and stearoyl-CoA desaturases in wild-type and *Elovl6*$^{-/-}$ mice (n=10). Error bars indicate SD. ND, not done. *, $P<0.05$; **, $P<0.01$; ***$P<0.001$.

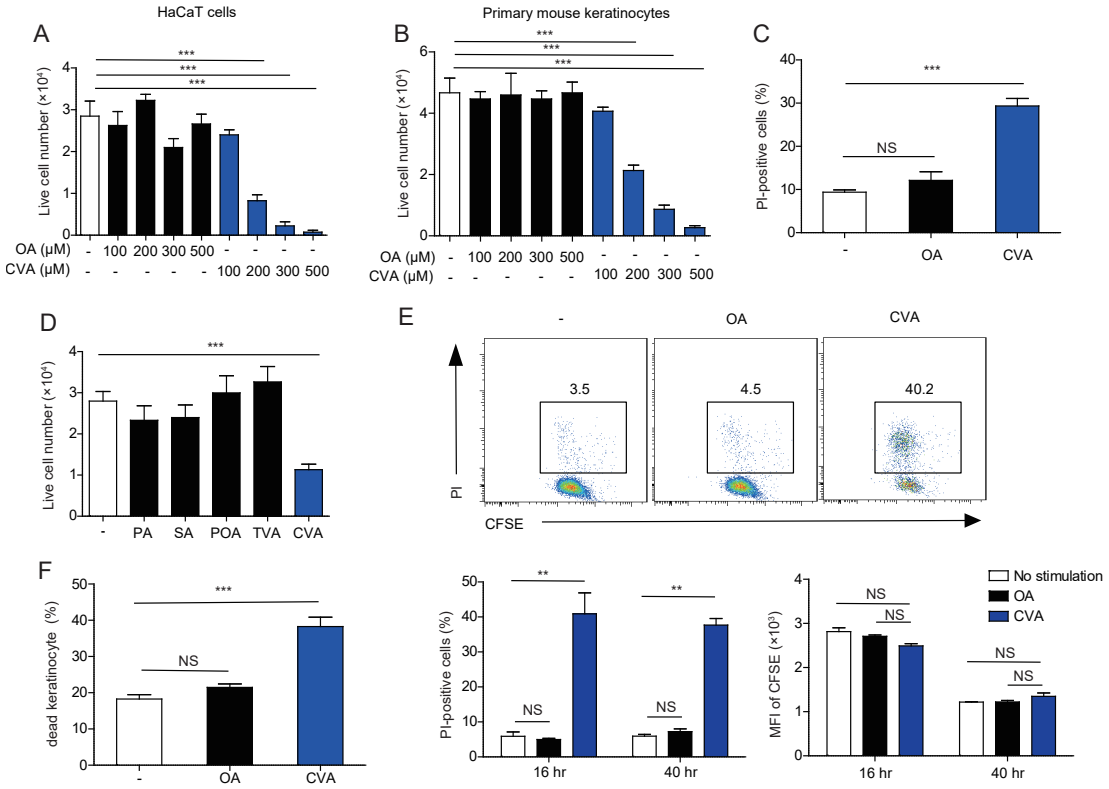

Fig. 5. Cis-vaccenic acid (CVA) induces keratinocyte death in the skin.

(A, B**,** D) Number of live cells in cultures of HaCaT cells (A) and primary keratinocytes (B, D) 16 h after stimulation with the indicated concentration of fatty acids (A, B) or with 300 μM of the indicated fatty acid (D) (n = 3 per group). (C) Primary keratinocytes were stimulated for 6 h with 300 μM of the indicated fatty acid and analyzed for propidium iodide (PI)-positive (i.e. dead) cells by flow cytometry (n = 4 or 5 per group). (E) HaCaT cells were labeled with 5-(and 6)-carboxyfluorescein diacetate succinimidyl ester（CFSE）and stimulated or not with 300 μM of OA or CVA for 16 h or 40 h. Cells were then stained with propium iodide (PI) and analyzed by flow cytometry. (**F**) Flow cytometry of epidermal cells isolated from the skin of wild-type mice that received topical application of ethanol (control) or 45mM of OA or CVA to the dorsal skin for 6 h (n = 6 per group). Error bars indicate SD. **, $P<0.01$; ***, $P<0.001$.

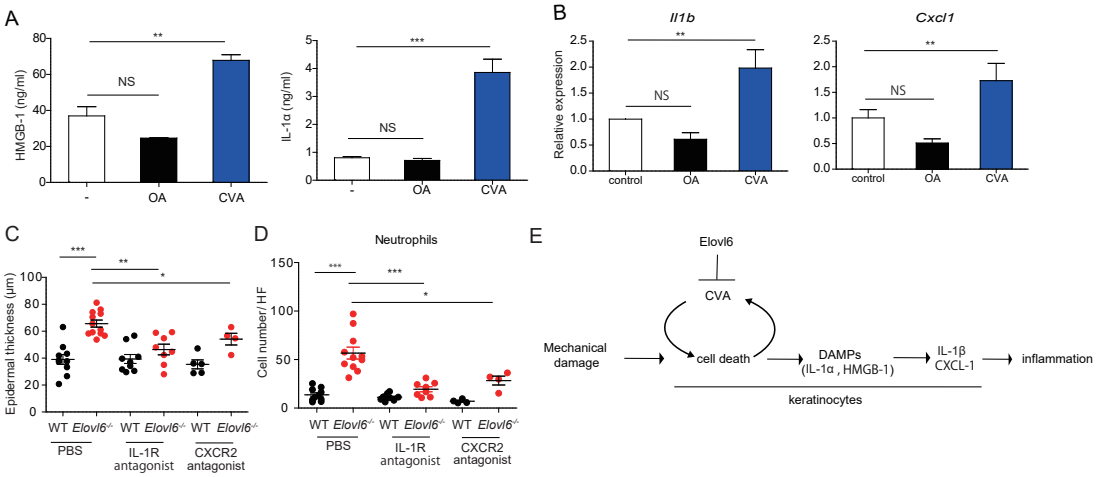

Fig. 6. CVA increased IL-1β and CXCL-1 production.

(A) Enzyme-linked immunosorbent assay of HMGB-1 (n = 4 per group) and cytokine bead array of IL-1α (n = 3 per group) in the supernatant of cultured primary keratinocytes 10 h after initiation of stimulation with 300 μM OA or CVA. (B) Quantitative RT-PCR analysis of *Il1β* and *Cxcl1* in the epidermis of wild-type mice 6 h after topical application of ethanol (control) (n = 10) or 15mM of OA (n = 13) or CVA (n = 14) (B). (C, D) Wild-type and *Elovl6*$^{-/-}$ mice were treated with PBS (n = 10 and 12, respectively), an IL-1 receptor antagonist (n = 9 and 8, respectively), or a CXCR-2 antagonist (n = 5 and 4, respectively) daily for 9 days, from the beginning on the day of tape stripping. Epidermal thickness (C) and the number of infiltrating neutrophils (D) were analyzed on day 9. (E) A proposed signal pathway from mechanical damage onto the skin to skin inflammation. Error bars indicate SD; *, $P < 0.05$; **, $P < 0.01$, ***, $P < 0.001$; NS, not significant. Data are representative of at least two independent experiments.

693 **Supplementary Figures**

694

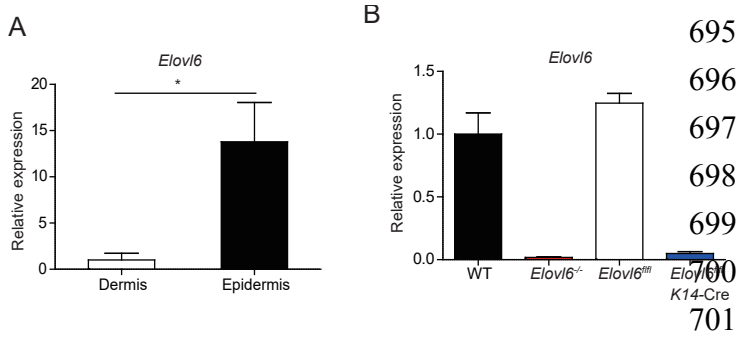

695 696 697 698 699 700 701

702 **Fig. S1. Expression of *Elovl6*.**

703 Quantitative RT-PCR analysis of *Elovl6* from dermis and epidermis (n = 3 per group)
704 (**A**) and from the epidermis of wild-type (WT), *Elovl6*$^{-/-}$, *Elovl6*$^{fl/fl}$, Elovl6$^{fl/fl}$ *K14*-Cre
705 mice (n=3 to 5 in each group) (**B**). Error bars indicate SD. **P*<0.05. Data are
706 representative of more than two independent experiments.

707

708

709

710

711

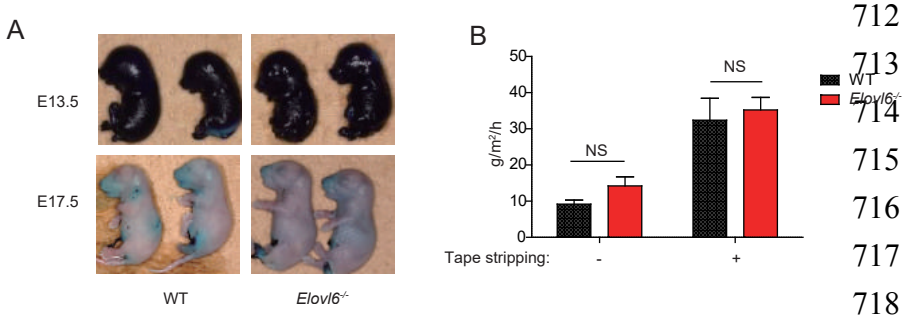

712 713 714 715 716 717 718 719

720 **Fig. S2. Comparable skin permeability barrier function between wild-type (WT)**
721 **and *Elovl6*$^{-/-}$ mice.**
722 (**A**) The fetuses at E13.5 and E17.5 from WT and *Elovl6*$^{-/-}$ mice were stained with 0.1%
723 toluidine blue for 24 h and photographed. (B) The transepidermal water loss of 6-8
724 weeks old WT and *Elovl6*$^{-/-}$ mice was measured before and after tape stripping (n = 14).
725 Error bars indicate SD. NS, not significant. Data are representative of three independent
726 experiments.

727

728

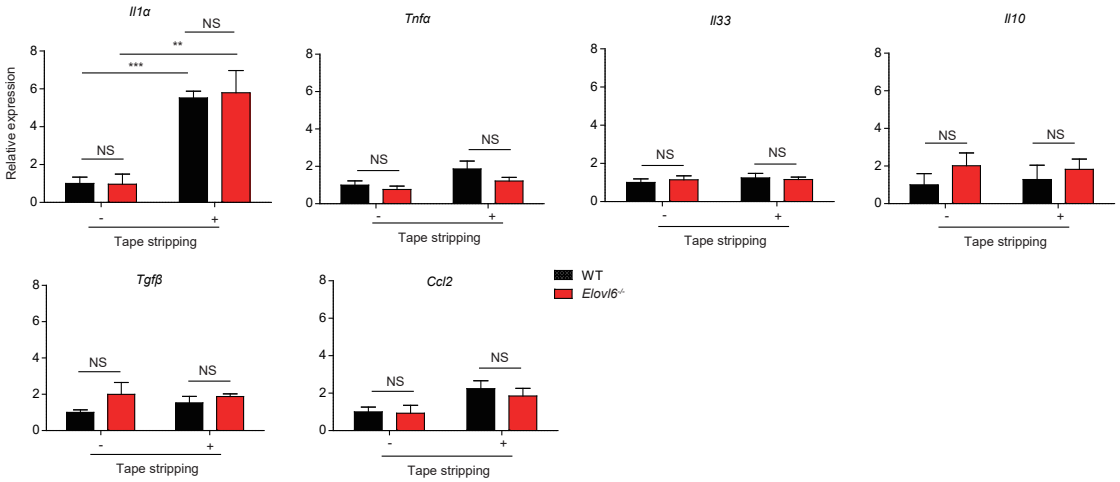

Fig. S3. Expression of cytokines

Quantitative RT-PCR analysis of the epidermis isolated before and 12 h after tape stripping from WT and *Elovl6*$^{-/-}$ mice and cultured for 24 h (n = 11 in each group). Error bars indicate SD. NS, not significant. ***P*<0.01, ****P*<0.001. Data are representative of two independent experiments.

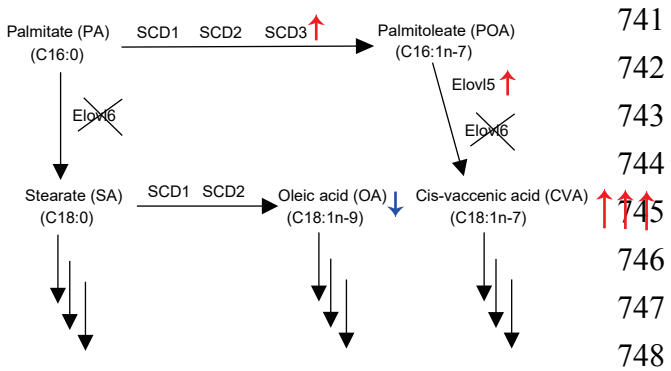

Fig. S4. Schematic representation of the proposed pathway (black arrows) controlling cis-vaccenic acid (CVA) generation in *Elovl6*$^{-/-}$ keratinocyte.

Red and blue arrows indicate the increase in SCD3, Elovl5, and CVA and the decrease in OA, respectively.

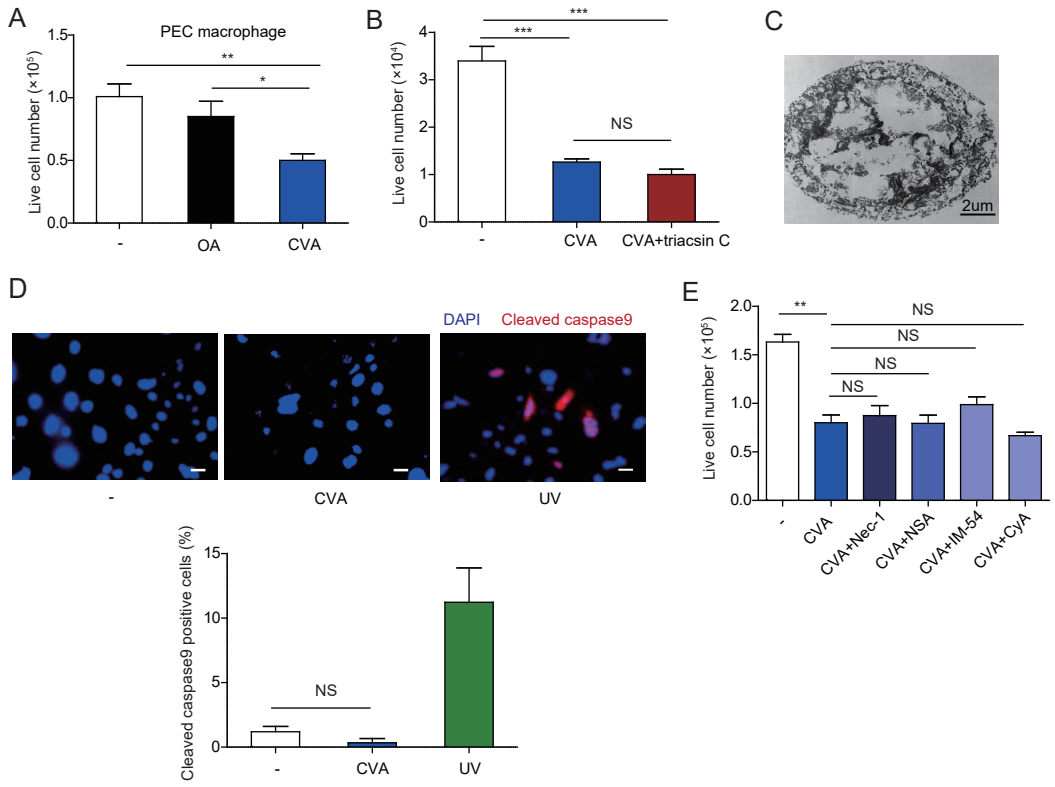

Fig. S5. CVA induced non-programmed cell death.

(A) Live cell number of primary peritoneal macrophages 16 h after stimulation with oleic acid (OA) or CVA (300 μM) (n = 3 in each group). (B**,** E) Primary mouse keratinocytes were cultured for 6 h in the presence or absence of 10 μM of triacsin C (B), or 1 mM necrostatin (Nec-1), 1 mM necrosulfonamide (NSA), 2 mM IM-54, or 1 mM cyclosporine (CyA) (E), followed by stimulation by adding 300 μM CVA; live cells were counted 16 h afterward (n = 3). (C) A representative dead primary keratinocyte induced by stimulation with 300 μM CVA for 10 h under a transmission electron microscope. (D) Immunofluorescence microscopic study of primary keratinocyte 10 h after stimulation with CVA or 6 h after ultraviolet irradiation. Cells were stained with anti-cleaved caspase 9, followed by Alexa Fluor 594-conjugated secondary antibody and DAPI. White bars indicate a scale (20 μm). Percentage of cleaved caspase 9-positive cells was calculated (n = 3). Error bars indicate SD. NS, not significant. *, $P<0.05$; **, $P<0.01$; ***, $P<0.001$. Data are representative of more than two independent experiments.

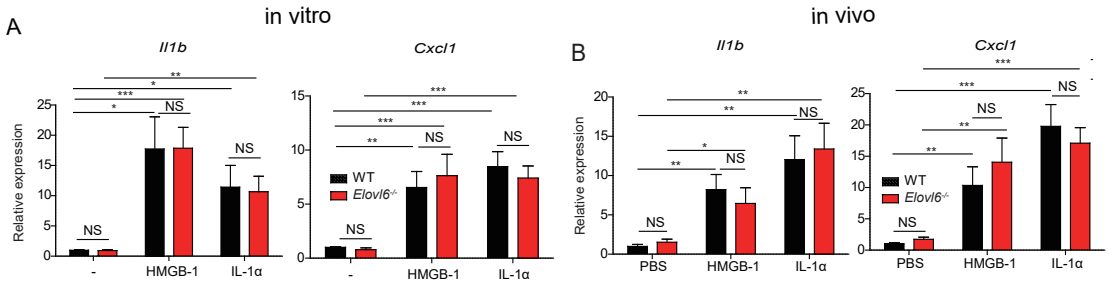

774

775 **Fig. S6. DAMPs increased IL-1β and CXCL-1 production.**

776 Quantitative RT-PCR analysis of *Il1β* and *Cxcl1* in keratinocytes of wild-type and

777 *Elovl6*$^{-/-}$ mice after stimulation or not with HMGB-1 or IL-1α in vitro (n=10 per group)

778 (A) and in the epidermis isolated 4 h after injection intradermally with PBS, HMGB-1,

779 or IL-1α (n = 8 per each group) (B).

780

781

782

783